Generated Pattern Current for Electrochemical Exfoliation: Intercalation Control, Flake Size Optimization, and Structural Quality Enhancement in Two-Dimensional Material Production

Ibrahim Karakoc

GigaPulse Energy, Izmir, Turkey | ibrahim@gigapulse.energy

PCT/TR2025/051176 | USPTO Appl. No. 19/298,223 | Priority Date: July 23, 2025

Abstract

Electrochemical exfoliation of layered crystal materials — graphite, MoS_2, WS_2, hexagonal boron nitride (hBN), and MXene precursors — provides a scalable route to two-dimensional (2D) nanosheets. The process proceeds through three sequential physical stages: anion intercalation into the interlayer gallery, electrochemical gas generation that drives interlayer pressure, and mechanical layer separation driven by the combined electrostatic and gas expansion forces. Conventional constant current (CC) exfoliation applies a temporally invariant current that drives all three stages simultaneously and uncontrolled, producing small flakes with high defect density (Raman D/G ratio > 0.5) because the aggressive gas generation required for separation also creates structural damage through uncontrolled interlayer pressure spikes.

This paper presents the application of the Generated Pattern Current (GPC) paradigm, implemented through the Dynamic Defined Pattern Charging (DDPC) framework, to electrochemical exfoliation. GPC separates the three exfoliation stages into independently controlled temporal phases within a single current profile: a high-current intercalation phase that maximizes SO_4^{2-} (or other anion) insertion and d-spacing expansion; a mid-current gas generation phase that builds interlayer pressure progressively rather than impulsively; and a low-current relaxation phase that allows stress redistribution and controlled layer separation without mechanical fracture of the exfoliated flake. Jensen's inequality applied to the nonlinear relationship between current density and gas generation rate formally establishes that temporally structured current produces different time-averaged interlayer pressure dynamics than equivalent CC. Predicted outcomes include flake lateral size increase from <5 μm to >10 μm, Raman D/G ratio reduction from >0.5 to <0.3, improved few-layer yield, and preserved production rate at equal average current. The framework extends to MoS_2, WS_2, hBN, and MXene exfoliation through the same three-phase current architecture.

Keywords: Generated Pattern Current (GPC); Dynamic Defined Pattern Charging (DDPC); electrochemical exfoliation; graphene; two-dimensional materials; ion intercalation; flake size; Raman D/G ratio; MoS_2; MXene; interlayer pressure

1. Introduction

1.1 Two-Dimensional Materials and Electrochemical Exfoliation

The isolation of graphene by Novoselov and Geim in 2004 [2] initiated a materials revolution in which atomically thin layers of van der Waals-bonded crystals were recognized as exhibiting properties qualitatively different from their bulk counterparts. Graphene's exceptional carrier mobility, mechanical strength, and thermal conductivity [7] stimulated intensive effort to identify and produce other 2D materials including transition metal dichalcogenides (TMDs) such as MoS_2 and WS_2 [9], hexagonal boron nitride (hBN), and the MXene family produced by selective etching of MAX-phase precursors [10]. The properties of 2D materials depend critically on structural quality: lattice defects, layer number non-uniformity, and oxidation all degrade the exceptional properties that make 2D materials technologically valuable.

Electrochemical exfoliation offers a scalable, solution-processable route to 2D nanosheets that complements mechanical cleavage (high quality, low throughput) and liquid-phase sonication (moderate quality, moderate throughput) [6]. In electrochemical exfoliation, the bulk crystal serves as the anode in an electrolyte containing intercalatable anions; the applied current drives ion insertion into the interlayer gallery, followed by electrochemical gas generation that expands the interlayer spacing beyond the van der Waals cohesion limit, producing exfoliated nanosheets [3,4,5]. The process is inherently scalable because it is driven by electrical current rather than mechanical agitation, and the current can in principle be controlled precisely.

1.2 Three Quality-Limiting Phenomena in CC Exfoliation

Ion intercalation kinetics determine the extent of d-spacing expansion before gas generation begins. Insufficient intercalation produces incomplete gallery opening, requiring higher gas pressure for separation and resulting in mechanical fracture rather than clean layer peeling. Excess intercalation time under CC wastes charge without additional benefit once the gallery is saturated. The intercalation time constant τ_{int} depends on the anion diffusion coefficient D_{anion} in the interlayer gallery and the gallery half-thickness d:

$$\tau_{int} \sim d^2 / D_{anion}$$

For SO_4^{2-} in graphite at room temperature, $\tau_{int} \sim$ 10–100 ms for typical gallery dimensions. CC exfoliation cannot independently control the intercalation stage duration—the same current that drives intercalation also drives gas generation, preventing independent optimization [3,4].

Interlayer gas generation rate determines the interlayer pressure P_{gas} that drives layer separation. The gas generation rate r_{gas} is a nonlinear function of the applied current density j:

$$r_{gas} \propto j \cdot \exp(\alpha_{gas} \cdot F \cdot \eta_{gas} / RT)$$

where η_{gas} is the overpotential for electrolyte decomposition (SO_4^{2-} oxidation to SO_2 and O_2 in sulfate electrolytes). Under CC, r_{gas} is constant and P_{gas} builds continuously. When P_{gas} exceeds the van der Waals cohesion force $F_{vdW} \approx 0.3$ J/m² abruptly, the rapid pressure release fractures the exfoliating flake rather than peeling it cleanly, generating small fragments with high edge defect density [3,5].

Layer separation mechanics determine the final flake size and structural integrity. Clean separation requires that the interlayer pressure P_{gas} builds gradually to slightly above the cohesion threshold while the intercalated gallery remains fully saturated with anions. CC

exfoliation cannot provide this graduated pressure profile because the gas generation rate is fixed by the constant current; any current high enough to drive separation at a practical rate also generates gas fast enough to cause mechanical fracture [4,5].

1.3 Limitations of CC and Pulsed Exfoliation

CC exfoliation applies a fixed anodic current that simultaneously drives intercalation, gas generation, and layer separation at rates determined by the single current setpoint. Increasing j improves production rate but worsens mechanical fracture; decreasing j reduces fracture but also reduces gas generation below the threshold needed for separation. The result is a fundamental tradeoff between production rate and flake quality that cannot be resolved within the CC paradigm.

Pulsed exfoliation with fixed on-off duty cycles has been explored and provides some improvement over CC by introducing periodic current-off intervals that allow partial stress relaxation [5]. However, fixed-parameter pulsing does not distinguish between the intercalation, gas generation, and separation stages, which occur at different timescales and require different current levels. GPC addresses this limitation by providing independent current control for each stage within a single pattern cycle.

1.4 GPC as Temporal Current Design for Exfoliation

Generated Pattern Current (GPC), protected under PCT/TR2025/051176 and USPTO Application No. 19/298,223 (priority date July 23, 2025), applies a three-phase temporal anodic current profile that independently addresses each exfoliation stage. The theoretical foundation derives from Jensen's inequality applied to the nonlinear relationship between current density and gas generation rate:

$$f(\bar{I}) \neq \langle f(I(t)) \rangle$$

where f represents the nonlinear gas generation rate r_gas(j). Because r_gas is a superlinear function of j (due to the exponential Butler-Volmer dependence on overpotential), the time-averaged gas generation rate under a structured current profile that includes both high-current and low-current phases differs substantially from r_gas at the time-averaged current. GPC exploits this nonlinearity to build interlayer pressure gradually and controllably rather than abruptly.

2. Electrochemical Exfoliation Physics

2.1 Van der Waals Cohesion and Separation Criterion

Layered crystals are held together by van der Waals (vdW) interlayer forces. The cohesion energy per unit area $E_{vdW} \approx 0.3$ J/m² for graphite establishes the minimum interlayer pressure-area product required for separation [6,7]. Layer separation occurs when:

$$P_{gas} \cdot A_{bubble} + F_{electrostatic} > F_{vdW} \cdot A_{flake}$$

where A_bubble is the cross-sectional area of the gas bubble nucleating at the intercalation front and A_flake is the area of the separating flake. The electrostatic force F_electrostatic from the electric field across the gallery contributes additionally during the high-field phases of GPC. The critical condition defines the minimum interlayer pressure required for separation, which in turn determines the minimum current required for gas generation sufficient to drive exfoliation [3,4].

2.2 Intercalation Kinetics and d-Spacing Dynamics

The intercalation process involves anion transport from the bulk electrolyte through the electrode surface into the interlayer gallery. For SO_4^{2-} intercalation into graphite in aqueous H_2SO_4 or $(NH_4)_2SO_4$ electrolyte, the d-spacing expands from 0.335 nm (pristine graphite) to approximately 0.79 nm upon stage-1 intercalation [3]. The d-spacing expansion follows:

$$\Delta d(t) = \Delta d_{max} \cdot (1 - \exp(-t/\tau_{int}))$$

where τ_{int} is the intercalation time constant and Δd_{max} is the maximum d-spacing expansion for the intercalant species. During the GPC high-current intercalation phase of duration t_{int}, the gallery expands progressively until Δd approaches Δd_{max}. The high-current phase must be maintained for $t_{int} \geq 2\tau_{int}$ to achieve near-complete gallery saturation before gas generation begins. Under CC, the intercalation and gas generation stages overlap because both are driven by the same continuous current, preventing gallery saturation before premature gas generation disrupts the intercalation front.

2.3 Electrochemical Gas Generation

In sulfate-based electrolytes ($(NH_4)_2SO_4$ or H_2SO_4), the primary gas-generating reactions at the graphite anode are:

$$SO_4^{2-} \rightarrow SO_2 + \tfrac{2}{2} O_2 + 2e^- \quad \text{(sulfate oxidation)}$$

$$H_2O \rightarrow \tfrac{1}{2} O_2 + 2H^+ + 2e^- \quad \text{(water oxidation)}$$

The gas generation rate per unit gallery area is:

$$r_{gas} = j/(zF) \cdot \eta_{Faradaic}$$

where z is the number of electrons transferred per gas molecule and $\eta_{Faradaic}$ is the Faradaic efficiency for gas production versus competing oxidation reactions. The interlayer pressure from generated gas:

$$P_{gas}(t) = n_{gas}(t) \cdot RT / V_{gallery}$$

where $V_{gallery}$ is the current interlayer gallery volume (a function of d-spacing) and $n_{gas}(t)$ is the cumulative moles of gas generated per unit area [4,5].

2.4 Flake Size and Defect Density Relationship

The lateral size of exfoliated flakes is inversely related to the density of fracture events during exfoliation. Each fracture event that propagates through the basal plane of a separating layer generates two new edge sites, each of which appears in the Raman spectrum as a D-band

contribution at ~1350 cm^{-1}. The Raman D/G intensity ratio therefore directly quantifies the density of in-plane defects created during exfoliation [8]:

$$D/G \propto N\_fracture / A\_flake$$

Under CC exfoliation, the abrupt pressure release when P_gas exceeds F_vdW drives rapid fracture propagation across the separating layer, producing many small fragments. Under GPC's graduated pressure buildup, the separation front advances progressively from the edge of the crystal inward, peeling large intact sheets without fracture.

3. Three-Phase GPC Exfoliation Model

3.1 Phase 1: Intercalation (High Current)

The GPC intercalation phase applies I_high for duration t_int = 2–3τ_int. During this phase, the anodic current drives rapid SO_4^{2-} transport into the interlayer gallery through electromigration and diffusion. The high current density creates a strong electric field gradient across the gallery that accelerates anion insertion beyond what diffusion alone would provide. The d-spacing expands from 0.335 nm toward Δd_max during t_int, while gas generation is minimized because the gallery is not yet saturated with intercalant and the electrolyte decomposition overpotential has not yet been reached.

The intercalation efficiency during Phase 1 is:

$$\eta\_int = \Delta d(t\_int) / \Delta d\_max \approx 1 - exp(-2\tau\_int/\tau\_int) = 1 - e^{-2} \approx 0.86$$

An 86% gallery saturation level before gas generation begins ensures that the subsequent pressure buildup occurs against a fully expanded gallery, maximizing the mechanical leverage for clean layer separation.

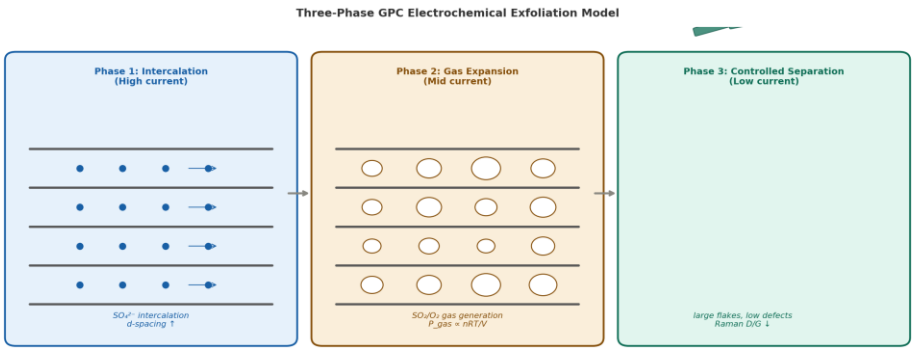

Figure 1. Three-phase GPC electrochemical exfoliation model: Phase 1 (high-current SO_4^{2-} intercalation, d-spacing expansion), Phase 2 (mid-current gas generation, interlayer pressure), Phase 3 (low-current controlled layer separation, large flakes).

Figure 1. Three-phase GPC electrochemical exfoliation model: Phase 1 (high-current SO_4^{2-} intercalation, d-spacing expansion), Phase 2 (mid-current gas generation, progressive interlayer pressure buildup), Phase 3 (low-current controlled layer separation with stress redistribution, large intact flakes).

3.2 Phase 2: Gas Expansion (Mid Current)

The GPC gas expansion phase applies I_mid ≈ 0.5–0.7·I_high for duration t_gas. During this phase, the current is reduced below the threshold for rapid electrolyte decomposition but maintained above the level needed for steady gas generation. The reduced current density

produces a lower gas generation rate r_gas,mid < r_gas,high, allowing P_gas to build gradually rather than impulsively. The progressive pressure buildup gives the gallery walls time to deform elastically rather than fracturing, distributing the mechanical stress uniformly across the separating layer.

Jensen's inequality applied to the superlinear r_gas(j) relationship:

$$\langle r\_gas(I(t)) \rangle\_GPC < r\_gas(I\_high) \quad during\ Phase\ 2$$

This means the time-averaged gas generation rate during Phase 2 is lower than at the Phase 1 current density, producing the desired gradual pressure buildup. The total gas generated over the GPC cycle is equal to the CC baseline (by Faraday's law at equal ⟨I⟩), but the temporal distribution of gas generation is fundamentally different: GPC produces sustained, moderate pressure rather than sudden, destructive pressure spikes.

3.3 Phase 3: Relaxation and Layer Separation (Low Current)

The GPC relaxation phase applies I_low ≈ 0.05–0.15·I_high for duration t_relax. During this phase, gas generation is nearly stopped while the accumulated interlayer pressure P_gas remains above the separation threshold F_vdW/A_flake. The pressure gradient drives progressive edge-to-center layer separation without mechanical fracture because the pressure is maintained just above the separation threshold rather than far above it. The relaxation phase also allows partial re-intercalation of ions at the newly exposed surfaces, which helps preserve the basal plane structure of the separating layer by filling vacancies created during intercalation.

The flake size achieved by GPC's relaxation phase scales with the time available for the separation front to propagate:

$$L\_flake \propto v\_front \cdot t\_relax$$

where v_front is the velocity of the separation front, which depends on the overpressure (P_gas − F_vdW/A_flake). At the low overpressure maintained by GPC's Phase 3, v_front is low and the front advances smoothly, producing large intact flakes. Under CC, the high overpressure drives rapid front propagation with simultaneous fracture, limiting flake size.

4. GPC Exfoliation Protocol Design

4.1 Three-Phase Current Architecture

The GPC electrochemical exfoliation protocol integrates the three stage-specific mechanisms into a composite current profile:

$$I(t) = I\_high\ [intercalation,\ t\_int] \rightarrow I\_mid\ [gas\ expansion,\ t\_gas] \rightarrow I\_low\ [relaxation,\ t\_relax]$$

The time-average constraint ⟨I(t)⟩ = I_dc is satisfied by design. Protocol parameter selection proceeds from characterization of the target material. The intercalation time constant τ_int is estimated from the d-spacing versus time curve measured by in-situ XRD or from the current

transient signature at constant voltage. I_high is set to maximize intercalation rate without initiating premature gas generation; I_mid is set to sustain steady gas generation just above the separation threshold; I_low is set to 5–15% of I_dc for stress redistribution without significant gas generation.

4.2 GigaPulse Lab Reference Implementation

The GigaPulse Lab platform serves as the reference implementation for GPC electrochemical exfoliation. GP Lab connects to the I and V control input terminals of the existing exfoliation power supply—no hardware replacement is required. Real-time feedback—measured anodic current I, cell voltage V, cell temperature T, and optionally acoustic emission as a proxy for mechanical fracture events—returns from the power supply to GP Lab for closed-loop control.

The platform's real-time analysis module tracks the cell voltage V signature during exfoliation: the onset of gas generation is indicated by a characteristic V plateau as the electrolyte decomposition overpotential is reached, and sudden layer separation events produce characteristic current spikes at constant voltage (or voltage drops at constant current). The decision engine uses these signatures to detect the transition between phases and adaptively adjust phase durations: when the intercalation signature is complete (d-spacing plateau in the V curve), Phase 2 is initiated; when the separation signature appears, Phase 3 begins to allow controlled relaxation.

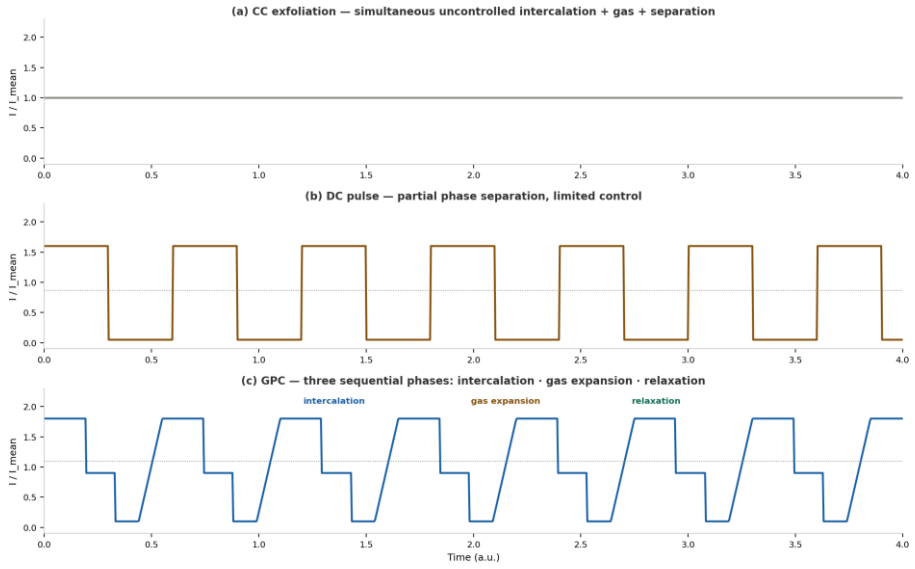

Figure 3. Current profile comparison: CC (constant, simultaneous uncontrolled phases), DC pulse (partial separation), and GPC three-phase pattern (intercalation · gas expansion · relaxation). All profiles share the same mean current ⟨I⟩.

Figure 2. Current profile comparison: CC exfoliation (constant, simultaneous uncontrolled intercalation + gas + separation), DC pulse (partial phase separation), and GPC three-phase pattern (intercalation · gas expansion · relaxation). All profiles share the same mean anodic current ⟨I⟩.

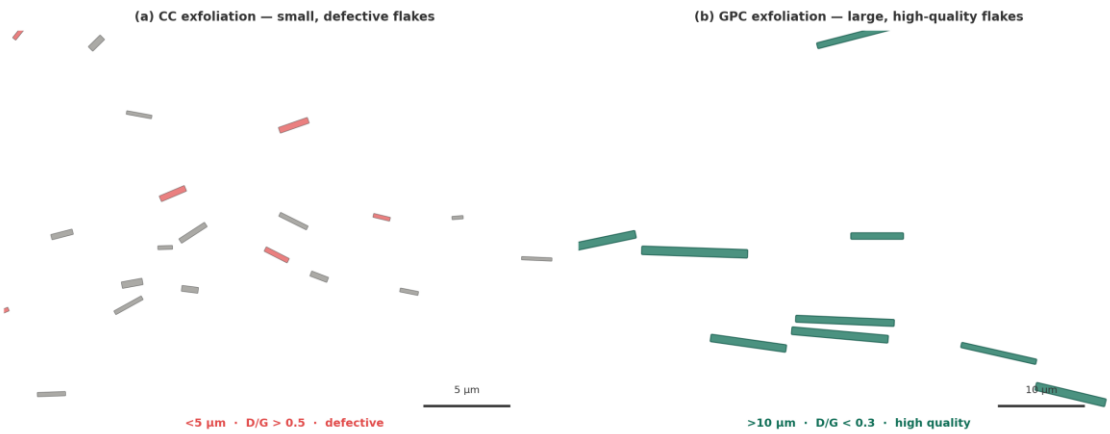

Figure 2. Exfoliation product comparison (schematic SEM): CC exfoliation (small, defective flakes, high Raman D/G ratio) vs GPC exfoliation (large, uniform flakes, low D/G ratio).

Figure 3. Exfoliation product comparison (schematic): CC exfoliation (small, defective flakes, high Raman D/G ratio) vs GPC exfoliation (large, uniform flakes, low D/G ratio, improved few-layer yield).

5. Extension to Other 2D Materials

5.1 Transition Metal Dichalcogenides (MoS_2, WS_2)

MoS_2 and WS_2 electrochemical exfoliation in Li^+-containing electrolytes proceeds through Li^+ intercalation followed by water-induced H_2 gas generation [9]. The three-stage GPC model applies directly: Phase 1 drives Li^+ intercalation and partial reduction of the 2H→IT structural phase transition; Phase 2 controls H_2 generation rate through the $I{\cdot}H_2O \rightarrow LiOH + \frac{1}{2}H_2$ reaction; Phase 3 allows controlled layer peeling and partial re-oxidation to recover the semiconducting 2H phase. GPC's Phase 3 relaxation is particularly important for MoS_2 because the 2H→IT phase transition is partially reversible during low-current relaxation, allowing recovery of semiconducting properties that are destroyed by the metallic IT phase under CC exfoliation.

5.2 Hexagonal Boron Nitride

hBN electrochemical exfoliation in molten salt or organic electrolytes is more challenging than graphite because the larger interlayer cohesion energy (~0.5 J/m² vs 0.3 J/m² for graphite) requires higher gas pressure for separation [6]. GPC's intercalation phase must achieve more complete gallery saturation before gas generation to avoid fracture. The longer intercalation time constant of hBN ($\tau_{int,hBN} > \tau_{int,graphite}$ due to the more corrugated interlayer surface) requires longer t_{int} in Phase 1. GPC's adaptive phase-transition detection automatically accommodates this material-specific difference.

5.3 MXene Precursor Exfoliation

MXene production involves selective etching of the A-layer from MAX-phase precursors (e.g., $Ti_3AlC_2 \rightarrow Ti_3C_2T_x$) followed by delamination [10]. The delamination step—separation of the MXene layers after A-layer removal—proceeds through intercalation of dimethyl sulfoxide (DMSO) or other intercalants followed by sonication. Electrochemical delamination using

GPC could replace or supplement mechanical sonication, with Phase 1 driving intercalant insertion, Phase 2 generating interlayer pressure through electrochemical reactions at the MXene surface, and Phase 3 providing controlled separation. The GigaPulse Lab application-specific calibration files encode the material-specific intercalation time constants and separation thresholds for each MXene composition.

6. Expected Outcomes

Parameter	CC exfoliation	GPC exfoliation
Flake lateral size	<5 μm	↑ >10 μm
Raman D/G ratio	>0.5 (high defects)	↓ <0.3 (low defects)
Few-layer yield (≤3L)	Reference	↑ Increased
Layer number uniformity	Heterogeneous	↑ Improved
Production rate	Reference	Preserved (same ⟨I⟩)
Mechanical fracture events	Frequent	↓ Suppressed
Ψ_GP,exfol quality factor	1.0	1.5–2.0× (flake area)

Table 1. Predicted GPC exfoliation outcomes compared to CC baseline at equal average anodic current density and equal production rate.

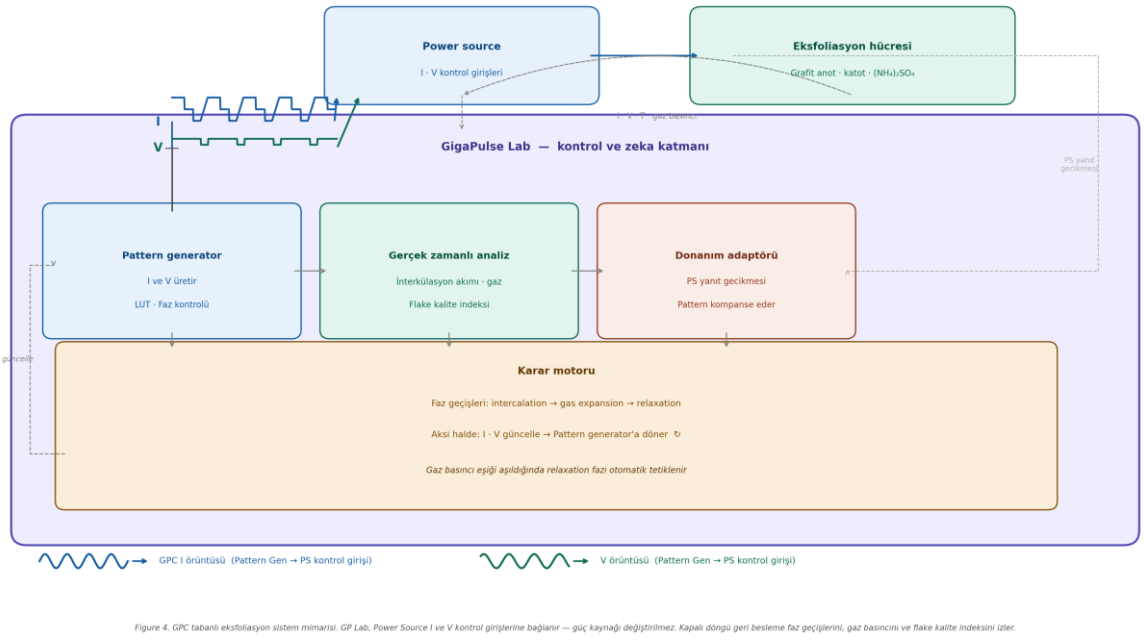

Figure 4. GPC tabanlı eksfoliasyon sistem mimarisi. GP Lab, Power Source I ve V kontrol girişlerine bağlanır — güç kaynağı değiştirilmez. Kapalı döngü geri besleme faz geçişlerini, gaz basıncını ve flake kalite indeksini izler.

Figure 4. GPC-based electrochemical exfoliation system architecture. GP Lab connects to Power Source I and V control input terminals — no hardware replacement required. Real-time feedback (I, V, T) enables closed-loop phase transition detection and adaptive pattern execution.

7. Experimental Validation Framework

7.1 Proposed Protocol

Independent experimental validation requires parallel comparison of CC and GPC exfoliation protocols applied to identical graphite anode materials in identical electrolytes with equal average current density and equal total charge passed. The primary measurement suite includes: Raman spectroscopy for D/G ratio and 2D/G ratio (layer number proxy); AFM for flake thickness distribution (layer count); SEM for lateral size distribution; TEM for lattice defect imaging; XPS for surface chemistry and oxidation state; and UV-vis absorbance spectroscopy for concentration estimation of exfoliated suspension.

Graphite foil anode in 0.1 M $(NH_4)_2SO_4$ aqueous electrolyte at +10 V vs Ag/AgCl provides a well-characterized model system with established CC literature baselines [3,4,5]. The GPC pattern parameters (t_int, t_gas, t_relax, I_high, I_mid) are systematically varied to map the parameter space of quality improvement as a function of the dimensionless ratios t_int/τ_int and I_high/I_mid.

7.2 GigaPulse Lab Integration

GPC electrochemical exfoliation is directly implementable on existing exfoliation setups without modification of the electrochemical cell, electrolyte, or electrode materials. GP Lab connects to the I and V control terminals of the existing potentiostat or galvanostat. The phase-transition detection algorithm—monitoring the V transient signature of intercalation completion and gas generation onset—provides material-specific adaptive control that eliminates the need for manually optimized fixed-parameter pulse protocols for each new material system.

8. Discussion

8.1 GPC Exfoliation in the Context of the 2D Materials Production Landscape

The three primary routes to 2D nanosheets—mechanical cleavage, liquid-phase sonication, and electrochemical exfoliation—represent a tradeoff between quality and throughput. Mechanical cleavage produces the highest quality material (single crystals, low defect density) but is limited to research quantities. Liquid-phase sonication achieves moderate throughput but produces small flakes with moderate defect density. Electrochemical exfoliation can in principle achieve high throughput with better quality control than sonication, but the CC paradigm has limited the achievable flake size and structural quality.

GPC repositions electrochemical exfoliation on the quality-throughput tradeoff curve by decoupling the intercalation, gas generation, and separation stages. The predicted flake size increase from <5 μm to >10 μm, combined with Raman D/G ratio reduction from >0.5 to <0.3, would bring GPC exfoliation quality into the range achievable by liquid-phase sonication while maintaining the throughput advantage of electrochemical methods. This is significant for applications requiring large-area, low-defect graphene films for transparent electrodes, barrier coatings, and composite reinforcement.

8.2 GPC Universality Across Layered Materials

The three-phase GPC exfoliation model applies to any layered crystal material for which electrochemical intercalation and gas generation are the driving forces for separation. The model parameters—intercalation time constant τ_int, gas generation overpotential threshold, and separation threshold pressure—are material-specific but can be extracted from standard electrochemical characterization (chronoamperometry, cyclic voltammetry, in-situ XRD) without material-specific model development. The GigaPulse Lab calibration file approach encodes these parameters for each material-electrolyte combination, enabling the same control platform to be applied across graphene, MoS_2, WS_2, hBN, and MXene production without hardware changes.

9. Conclusion

This paper has established the theoretical framework for applying Generated Pattern Current to electrochemical exfoliation of layered crystal materials. The fundamental limitation of CC exfoliation—simultaneous, uncontrolled driving of intercalation, gas generation, and layer separation at rates determined by a single current setpoint—is overcome by GPC's three-phase temporal current design. Jensen's inequality applied to the superlinear gas generation rate kinetics establishes that temporally structured current produces different time-averaged interlayer pressure dynamics than equivalent CC, enabling graduated pressure buildup that drives clean layer separation rather than mechanical fracture.

The three GPC phases independently optimize each exfoliation stage: high-current Phase 1 maximizes intercalation completeness before gas generation begins; mid-current Phase 2 builds interlayer pressure progressively; low-current Phase 3 allows stress redistribution and clean layer peeling. Predicted improvements—flake lateral size >10 μm, Raman $D/G < 0.3$, improved few-layer yield—at preserved production rate represent a significant advance for electrochemical 2D material production. The framework extends naturally to MoS_2, WS_2, hBN, and MXene through the same three-phase architecture.

References

[1] I. Karakoc, "Dynamic Defined Pattern Charging (DDPC)," PCT/TR2025/051176; USPTO 19/298,223. Priority: July 23, 2025.

[2] K. S. Novoselov et al., "Electric Field Effect in Atomically Thin Carbon Films," Science, vol. 306, pp. 666–669, 2004.

[3] K. Parvez et al., "Exfoliation of Graphite into Graphene in Aqueous Solutions of Inorganic Salts," J. Am. Chem. Soc., vol. 136, pp. 6083–6091, 2014.

[4] K. Parvez et al., "Electrochemically Exfoliated Graphene as Solution-Processable, Highly Conductive Electrodes for Organic Electronics," ACS Nano, vol. 7, pp. 3598–3606, 2013.

[5] S. Yang et al., "Organic Radical-Assisted Electrochemical Exfoliation for the Scalable Production of High-Quality Graphene," J. Am. Chem. Soc., vol. 137, pp. 13927–13932, 2015.

[6] J. N. Coleman et al., "Two-Dimensional Nanosheets Produced by Liquid Exfoliation of Layered Materials," Science, vol. 331, pp. 568–571, 2011.

[7] A. H. Castro Neto et al., "The Electronic Properties of Graphene," Rev. Mod. Phys., vol. 81, pp. 109–162, 2009.

[8] A. C. Ferrari et al., "Raman Spectrum of Graphene and Graphene Layers," Phys. Rev. Lett., vol. 97, p. 187401, 2006.

[9] M. Chhowalla et al., "The Chemistry of Two-Dimensional Layered Transition Metal Dichalcogenide Nanosheets," Nat. Chem., vol. 5, pp. 263–275, 2013.

[10] M. Naguib et al., "Two-Dimensional Nanocrystals Produced by Exfoliation of Ti_3AlC_2," Adv. Mater., vol. 23, pp. 4248–4253, 2011.

[11] A. J. Bard and L. R. Faulkner, Electrochemical Methods: Fundamentals and Applications, 2nd ed., Wiley, 2001.

[12] J. Newman and K. E. Thomas-Alyea, Electrochemical Systems, 3rd ed., Wiley, 2004.

[13] X. Wang et al., "Electrochemical Exfoliation of Graphite into Graphene in Acidic Solutions," Chem. Commun., vol. 50, pp. 10989–10992, 2014.

[14] C. T. J. Low et al., "Electrochemical Approaches to the Production of Graphene Flakes and Their Potential Applications," Carbon, vol. 54, pp. 1–21, 2013.

[15] Y. Huang et al., "An Innovative Way for the Mass Production of Graphene," Small, vol. 11, pp. 1392–1401, 2015.

[16] Z. Y. Xia et al., "The Exfoliation of Graphene in Liquids by Electrochemical, Chemical, and Sonication-Assisted Techniques: A Nanoscale Study," Adv. Funct. Mater., vol. 23, pp. 4684–4693, 2013.

[17] J. M. Tour, "Top-Down versus Bottom-Up Fabrication of Graphene-Based Electronics," Chem. Mater., vol. 26, pp. 163–171, 2014.

[18] D. Voiry et al., "Enhanced Catalytic Activity in Strained Chemically Exfoliated WS_2 Nanosheets," Nat. Mater., vol. 12, pp. 850–855, 2013.

[19] M. Osada and T. Sasaki, "Two-Dimensional Dielectric Nanosheets: Novel Nanoelectronics from Nanocrystal Building Blocks," Adv. Mater., vol. 24, pp. 210–228, 2012.

[20] B. Anasori, M. R. Lukatskaya, and Y. Gogotsi, "2D Metal Carbides and Nitrides (MXenes) for Energy Storage," Nat. Rev. Mater., vol. 2, p. 16098, 2017.

[21] R. Mas-Ballesté et al., "2D Materials: To Graphene and Beyond," Nanoscale, vol. 3, pp. 20–30, 2011.

[22] F. Withers et al., "Light-Emitting Diodes by Band-Structure Engineering in van der Waals Heterostructures," Nat. Mater., vol. 14, pp. 301–306, 2015.

[23] A. K. Geim and I. V. Grigorieva, "Van der Waals Heterostructures," Nature, vol. 499, pp. 419–425, 2013.

[24] G. Fiori et al., "Electronics Based on Two-Dimensional Materials," Nat. Nanotechnol., vol. 9, pp. 768–779, 2014.

[25] S. Z. Butler et al., "Progress, Challenges, and Opportunities in Two-Dimensional Materials Beyond Graphene," ACS Nano, vol. 7, pp. 2898–2926, 2013.

Acknowledgments

The GPC-based electrochemical exfoliation protocol is protected under PCT/TR2025/051176 and USPTO Application No. 19/298,223. The author is the named inventor. No external funding was received for the preparation of this manuscript.

Declaration of Competing Interest

Ibrahim Karakoc holds intellectual property and commercial rights related to the Generated Pattern Current (GPC) and Dynamic Defined Pattern Charging (DDPC) technology described in this paper through GigaPulse Energy, Izmir, Turkey.

Data Availability

Data will be made available on request.

Declaration on the Use of AI Writing Assistance

The author used AI-assisted writing tools for language editing and manuscript preparation. The scientific content, theoretical analysis, and all intellectual contributions are entirely the work of the author.